sustainable chemistry

MDPI

*Article*

# Sodium-Oxide Fluxed Aluminothermic Reduction of Manganese Ore for a Circular Economy: Cr Collector Metal Application

**Theresa Coetsee [1,*] and Frederik De Bruin [2]**

[1] Department of Materials Science and Metallurgical Engineering, University of Pretoria, Pretoria 0002, South Africa
[2] Independent Metallurgical Consultant, Pretoria 0002, South Africa; fjdb.1953@gmail.com
* Correspondence: theresa.coetsee@up.ac.za

## Abstract

Aluminothermic reduction is gaining renewed interest as an alternative processing route for the circular economy. Aluminium is produced electrochemically in the Hall–Héroult process with minimal $CO_2$ emissions if electricity is sourced from non-fossil fuel energy sources. The $Al_2O_3$ product from the aluminothermic reduction process can be recycled via hydrometallurgy, with leaching as the first step. $NaAlO_2$ is a water-leachable compound that forms a pathway for recycling $Al_2O_3$ with hydrometallurgy. In this work, a suitable slag formulation is applied in the aluminothermic reduction of manganese ore to form a $Na_2O$-based slag of high $Al_2O_3$ solubility to effect good alloy–slag separation. The synergistic effect of added chromium metal as a collector metal is illustrated with an increased alloy yield at 68%, from 43% without added Cr. The addition of small amounts of carbon reductant to $MnO_2$-containing ore ensures rapid pre-reduction to MnO. This approach negates the need for a pre-roasting step. The alloy and slag chemical analyses are compared to the thermochemistry-predicted phase chemistry. The alloy consists of 57% Mn, 18% Cr, 18% Fe, 3.4% Si, 1.5% Al, and 2.2% C. The formulated slag exhibits high $Al_2O_3$ solubility, enabling effective alloy–slag separation, even at an $Al_2O_3$ content of 55%.

**Keywords:** aluminothermic; circular economy; reductant; ferroalloy; sustainable; chromium; manganese ore; medium carbon



Academic Editor: Matthew Jones

Received: 9 August 2025
Revised: 15 September 2025
Accepted: 16 September 2025
Published: 18 September 2025

**Citation:** Coetsee, T.; De Bruin, F. Sodium-Oxide Fluxed Aluminothermic Reduction of Manganese Ore for a Circular Economy: Cr Collector Metal Application. *Sustain. Chem.* **2025**, *6*, 30. https://doi.org/10.3390/suschem6030030



## 1. Introduction

Thermic reduction of oxides with Al or Si as reductant is a well-established method for producing low-carbon ferroalloys. Both ferromanganese and ferrochromium of low carbon content can be produced in this way [1]. In the production of low-carbon ferrochromium (LCFeCr) and medium-carbon ferrochromium (MCFeCr) via silicothermic reduction, the Si reductant is applied in the form of ferrosilicon or ferrosilicochromium (45% Si, 40% Cr, 0.02% C) [1]. Typical ferrochromium grades are summarised in Table 1 to indicate the %C ranges per category of ferrochromium [1–3]. There are also sub-categories with lower %Cr; for example, as low as 45% Cr is deemed acceptable [1]. MCFeCr can be produced by silicothermic reduction or by refining high-carbon ferrochromium (HCFeCr) in the oxygen-blown converter process [1]. The slag used as a reactant feed in the silicothermic production process is prepared by melting a lime–chromite ore mixture in an electric furnace [1,3]. Similarly, to produce the Si reductant from quartz as ferrosilicon or ferrosilicochromium, an electric furnace is used. Consequently, the overall energy requirement for MCFeCr and LCFeCr production is high, at 8000–9000 kWh/t product [1].

**Table 1.** Ferromanganese alloy compositions (mass%): n.s. = not specified [1–3].

| | %Cr | %Si | %C | %S | %P | %Al | %Mn | Balance |
|---|---|---|---|---|---|---|---|---|
| HCFeCr (C) [2] | 62–72 | <3.0 | 4.0–9.5 | <0.060 | <0.030 | 0 | 0 | Fe |
| MCFeCr [1] | 65–75 | <1.5 | 0.5–4.0 | <0.050 | <0.030 | 0 | 0 | Fe |
| LCFeCr (D) [2] | 67–75 | <1.0 | <0.75 | <0.025 | <0.030 | 0 | 0 | Fe |
| Charge chrome [1] | 53–58 | 6–3 | 5–8 | n.s. | n.s. | 0 | 0 | Fe |
| FeCrAl [3] | 48–52 | 0.5–1 | 0 | 0 | 0 | 18–22 | 0 | Fe |
| FeCrMn [3] | 31–39 | <1.6 | <0.05 | 0 | 0 | 0 | 36–44 | Fe |
| FeCrSiMn [3] | 20–25 | 20–30 | <0.05 | <0.05 | <0.02 | 0 | 30–35 | Fe |

Aluminothermic reduction can also be used to produce low-carbon ferrochromium; however, it is historically considered too expensive [1]. A recent new interest has developed in sourcing Al reductant from industrial waste streams of ferroaluminosilicalcium (FeAlSiCa) and ferrosilicochrome (FeSiCr) dust to produce carbon-free ferrochrome [4,5]. Beketov pioneered the aluminothermic reduction process in 1859 [6]. In the 19th century, the cost of aluminium decreased sufficiently for the practical industrial application of aluminothermic reduction, via the work of Beketov and Goldschmidt, respectively [6]. Despite a long history of development of aluminothermic reduction, different research approaches are used to improve process understanding and optimise reactant utilisation. For example, some studies applied reactants under a protective gas atmosphere to study specific reactions [7–11], while others performed aluminothermy in air to study the real-life process with ignition in air [12–16]. Process simulation experiments should be performed in air to assess the feasibility of the process in terms of reactant consumption, temperature attainment, and slag–metal separation.

As described by Gasik, the complex ferroalloy of FeCrAl is useful since the Al serves as a deoxidiser element whilst the liquid steel is alloyed with Cr, resulting in limited oxidation loss of Cr [3]. Aluminothermic reduction in chromium oxide materials with an excess of Al added can be used to produce this alloy. Carbothermic reduction of fused alumina in the presence of ferrochrome or ferrosilicochrome in a ferroalloy furnace can also produce this alloy [3]. Similarly, complex alloys such as ferrochrome-manganese alloy (FeCrMn) and ferrochrome-siliconmanganese alloy (FeCrMnSi) may be produced by reducing chromium and manganese oxide-containing melts with silicon and/or carbon reductant [3]. The motivation for using FeCrMn alloy as an alloying source addition to liquid steel is that the melting temperature is low (1400–1500 °C) in 30% Mn-35% Mn alloy, compared to the high melting temperature of LCFeCr (1640–1680 °C), and so facilitating fast dissolution into liquid steel [3]. A complex alloy for alloying high-carbon and tool steels is produced by high-temperature (1600–1700 °C) carbothermic reduction of low-grade manganese ore and chrome ore in an electric furnace. The reported average alloy composition is 19% Fe, 14% Si, 8% Mn, 58% Cr, 6% C [17]. The compositions of high manganese chromium-containing complex alloys are summarised in Table 1. From the above discussion, it is clear that a FeCrMnSiAl complex alloy may find similar application in liquid steel alloying.

Considering the shift in process requirements to reduce $CO_2$ emissions and apply circular economy principles in metals production, the application of Al is a possible alternative processing route because Al is produced electrochemically in the Hall–Héroult process. This processing approach limits $CO_2$ emissions if the electricity input is sourced from non-fossil fuel energy sources. This approach is attracting increased research attention in the aluminothermic production of manganese and silicon alloys, as well as in the recycling of waste streams, such as end-of-life lithium-ion batteries and waste iron oxides, including mill scale [7–10,12,13]. Furthermore, the $Al_2O_3$ product may be recycled as feed to the Hall–Héroult process after hydrometallurgical treatment [18,19]. Aluminothermic

reduction of manganese ore is already applied to produce low-carbon ferro-manganese alloy. The $MnO_2$ ore is pre-roasted to convert the $MnO_2$ to lower oxidation state oxides of $Mn_2O_3$ and $Mn_3O_4$ to prevent violent heat release from aluminothermic reduction of $MnO_2$ [15]. The ore feed requirement is a minimum of 46% Mn and a Mn/Fe ratio of 9, with a P content below 0.12%, and $CaF_2$ is added as a flux. The product alloy composition ranged from 70 to 84% Mn, 13–16% Fe, 1–10% Si, <0.03% Al, and <0.24% P, and the metal yield was 58–64% [15].

An essential aspect of aluminothermic reduction is the optimal separation of the produced alloy from the slag. Since $Al_2O_3$ has a high melting point, the slag chemistry must be designed to flux most of the $Al_2O_3$. Thus, slag volume can be excessive, and the phase chemistry of the slag will likely influence the ease of subsequent processing for $Al(OH)_3$ formation via hydrometallurgy. Since CaO and $Al_2O_3$ form low liquidus compounds and CaO in the slag increases the activity of MnO in the slag to promote the aluminothermic reduction of MnO, the aim slag of CaO-$Al_2O_3$ chemistry was applied [7,8]. Most of the Al was leached from CaO-$Al_2O_3$ slag in a 10% $Na_2CO_3$ solution, reacted at 30–45 °C [18]. A different approach is to use a $Na_2O$-$Al_2O_3$-based slag since the $NaAlO_2$ compound can be leached in water at 60 °C [19]. Adequate leaching conditions were identified at a solid–liquid ratio of 1:10 with a leaching time of 60 min at 60 °C. The leachate contained $Na^+$:$Al^{3+}$ at 1.43:1. Carbonation with $CO_2$ gas bubbled through the solution at 80 °C and resulted in a pH of 12.5–10.5 for 96.5% Al recovery as α-$Al(OH)_3$ (Bayerite) particles of 90% +44 μm and 98.8% alumina grade, suitable as feed to the Hall–Héroult process after calcination to α-$Al_2O_3$ [19].

The objective of this work is to produce a medium-carbon Mn-Cr-Fe alloy with a $Na_2O$-fluxed formulation for the circular aluminothermic reduction of manganese ore with chromium metal as the collector metal. A successful slag formulation must achieve high $Al_2O_3$ solubility to facilitate adequate alloy–slag separation. It must allow the $Al_2O_3$ product to be recovered via hydrometallurgy by forming the desired water-soluble compound, $NaAlO_2$.

## 2. Materials and Methods

The experimental details in this work are the same as in our previously reported work. In this work, Cr metal is applied as collector metal instead of the Si metal addition applied previously [16]. The addition of Si metal resulted in a high uptake of Si in the alloy, forming a bulk alloy of 1.4% Al, 8.7% Si, 65.8% Mn, 21.8% Fe, 2.2% C at 56% alloy yield.

### *2.1. Materials*

The reaction mixture consisted of manganese ore, coal, metal powders of aluminium and chromium, and lime and sodium silicate as flux. The chemically pure metal powders were sourced as follows: Al (99.7% Al, −1 mm) supplied by Sigma-Aldrich (Johannesburg, South Africa), and Cr (99.0% Cr, −44 μm) provided by Alfa Aesar (Johannesburg, South Africa). The chemically pure sodium silicate is supplied by Sigma-Aldrich (Johannesburg, South Africa), and CaO is provided by Associated Chemical Enterprises (Johannesburg, South Africa). The manganese ore is a pyrolusite ($MnO_2$)-based ore sourced from a small-scale ore body complex in South Africa, and the medium-volatile coal is also sourced from South Africa. The coal contains 22.5% volatile matter, 12% ash, 62.2% fixed carbon, and 3.3% moisture. Table 2 presents the analyses of ore and coal ash. The mixture, based on 100 g of ore, was placed in a graphite crucible and sealed with a graphite lid. The crucible dimensions were 50 mm inner diameter, 70 mm in height, and 7 mm in wall thickness. The lid was recessed by 7 mm to fit the crucible's inner diameter. The reaction mixtures are summarised in Table 3.

**Table 2.** Bulk chemical composition of manganese ore and coal ash (mass%).

| | %FeO | %MnO | %$Cr_2O_3$ | %$V_2O_5$ | %$TiO_2$ | %CaO | %$K_2O$ | %$P_2O_5$ | %$SiO_2$ | %$Al_2O_3$ | %MgO | %$Na_2O$ | %BaO |
|---|---|---|---|---|---|---|---|---|---|---|---|---|---|
| Ore | 10.70 | 61.59 | 0.03 | 0.04 | 0.05 | 0.23 | 0.21 | 0.01 | 5.43 | 2.61 | 0.11 | 0.00 | 1.85 |
| Ash | 1.51 | 0.02 | 0.05 | 0.05 | 2.16 | 2.46 | 0.51 | 1.19 | 51.44 | 39.35 | 0.68 | 0.30 | 0.27 |

**Table 3.** Reaction mixtures (grams).

| | Ore | Coal | $Na_2O{\cdot}SiO_2$ | CaO | Al | Cr |
|---|---|---|---|---|---|---|
| Base case (BC) | 100 | 27 | 20 | 15 | 0 | 0 |
| A | 100 | 10 | 20 | 15 | 30 | 0 |
| D | 100 | 10 | 20 | 15 | 30 | 10 |

## *2.2. Methods*

### 2.2.1. Experimental Procedure

The masses of the reaction mixture were weighed and mixed thoroughly in a mixing container. The mixture was transferred into the graphite crucible, and the graphite lid was placed onto the crucible rim. The muffle furnace was pre-heated and soaked for 12 h at the set-point temperature of 1350 °C. The proportional-integral-derivative (PID) controller was used to control the muffle furnace temperature. The aluminothermic reaction consists of placing the graphite crucible and contents into the muffle furnace. From prior experimentation, it was noted that the crucible must be removed from the furnace 2 min after ignition, marked by a flash flame exiting the muffle furnace's top side-panel joint gaps. Therefore, the reaction mixture was not entirely heated by the muffle furnace, but rather via the exothermic aluminium (aluminothermic) reactions. The ignition time was 6 min after placing the crucible in the furnace. Following a total reaction time of 8 min, the crucible and its contents were removed from the furnace. The lid was then removed, and the molten metal and slag were poured into a cast-iron mould. Upon cooling to room temperature, the poured contents were returned to the graphite crucible for manual separation of metal and slag.

### 2.2.2. Materials Analyses

The large slag and alloy blobs were sectioned for chemical analysis of the alloy and slag phases using a scanning electron microscope (SEM). The cross-section faces were coated with gold for analysis by the SEM via a Zeiss 540 Ultra FEG (field emission gun) SEM (Zeiss, Oberkochen, Germany) with energy dispersive X-ray spectroscopy (EDX) probe operated at 20 kV. Inductively coupled plasma optical emission spectroscopy (ICP-OES) method using a Perkin Elmer Optima 5300 instrument (Perkin Elmer, Springfield, IL, USA) was used in ore, bulk alloy, and slag analyses. The alloy carbon and sulphur content was analysed by the combustion method using a LECO CS 744 instrument (LECO, St Joseph, MO, USA). A proximate analysis of the coal was conducted in accordance with the South African National Standard (SANS 1726:2011) [20]. The coal ash was analysed by X-ray fluorescence (XRF) spectrometer using an ARL Advant'X Series Sequential Intellipower$^{TM}$ XRF instrument (Thermo Fisher Scientific, Waltham, MA, USA).

### 2.2.3. Thermochemical Calculations

The alloy equilibrium phase chemistries were calculated in Thermo-Calc 2023b software, using the SGTE Alloy 4.9 database [21]. The equilibrium phase chemistry of the target slag and the sample D slag was calculated in FactSage, as well as the gas–slag–metal equilibrium for the sample D inputs. The Equlib module in FactSage 7.3 was used with selecting the FToxid database and SGTE alloy database [22].

## 3. Results

Although the results of sample A with carbon and aluminium added have been shown elsewhere, for comparison, the sample A results are also presented here [16]. Similarly, a photograph of the base case (BC) sample is shown in Figure 1a to confirm that no significant slag or alloy formed at the low initial temperature in the muffle furnace (1350 °C). The magnetic fraction of this sample is shown in Figure 1a, with only sintered material formed and no slag or alloy mass formation. This effect is due to the absence of exothermic heat and fast reduction reactions from aluminothermic reduction. Carbothermic reduction is slower than aluminothermic reduction and is highly endothermic due to the endothermic Boudouard reaction, requiring non-chemical heating from the furnace. Therefore, a much longer dwell time in the furnace would be required to achieve noticeable alloy formation via carbothermic reduction. In contrast, large alloy blobs were effectively separated from the slag in samples A and D, along with some smaller metal droplets, as seen in Figure 1b,c. The alloy composition of the fractured surfaces of the large alloy volumes was analysed by SEM-EDX. A typical analysis area consisted of 0.5 mm × 0.5 mm. Figures 2 and 3 display the EDX element maps and SEM images of example areas comprising the field of view (FOV) from the regions analysed in samples A and D. The sample A alloy in Figure 2 appears to be a homogenous Mn-Fe-Si single-phase alloy. The sample D alloy contains small slivers of Cr in a homogeneous single-phase alloy of Mn-Fe-Si-Cr.

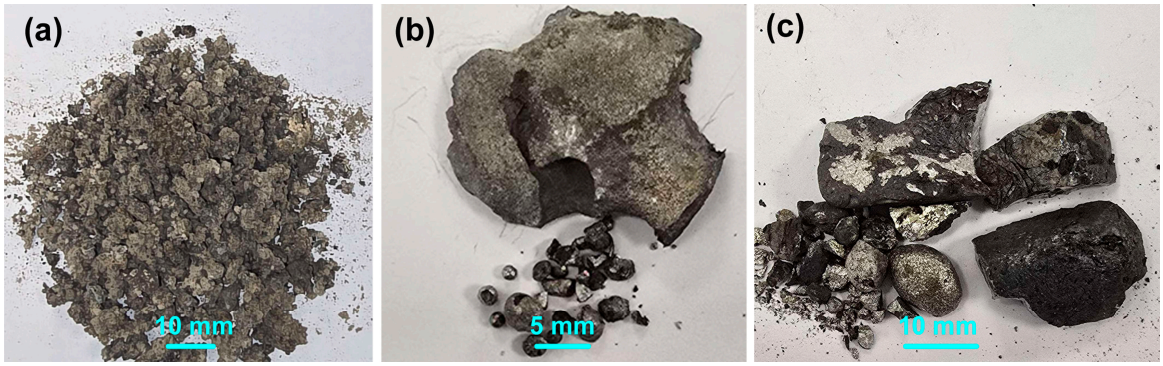


**Figure 1.** (**a**) Photographs of magnetic fraction from Sample BC; (**b**) easily separated alloy from Sample A; (**c**) easily separated alloy from Sample D.

The analyses of the areas are summarised in Tables 4 and 5. The analyses per area in each sample are closely matched. The maximum variance (σ) of the SEM-EDX analyses for each element is also indicated. The bulk chemistry of each alloy is also displayed in Tables 4 and 5, specifically, because the SEM-EDX does not accurately analyse for carbon, whilst the LECO combustion analysis of the bulk alloy provides quantitative %C. It is observed that the carbon in Figures 2 and 3 appears as specs on the surface of the sample and does not form part of the bulk alloy. The carbon specs were most likely formed from the decomposition of CO in the product gas as the material cooled down. Significant quantities of CO gas may form as shown in the gas–slag–metal equilibrium calculations in Section 4.3. However, most of the carbon is present in the bulk alloys, with the %C in the bulk sample A alloy as 3.5%, and in the sample D alloy it is 2.2%. Similarly, the Al appears as specs in Figures 2 and 3, although the analyses are at a level of approximately 1% in both samples.

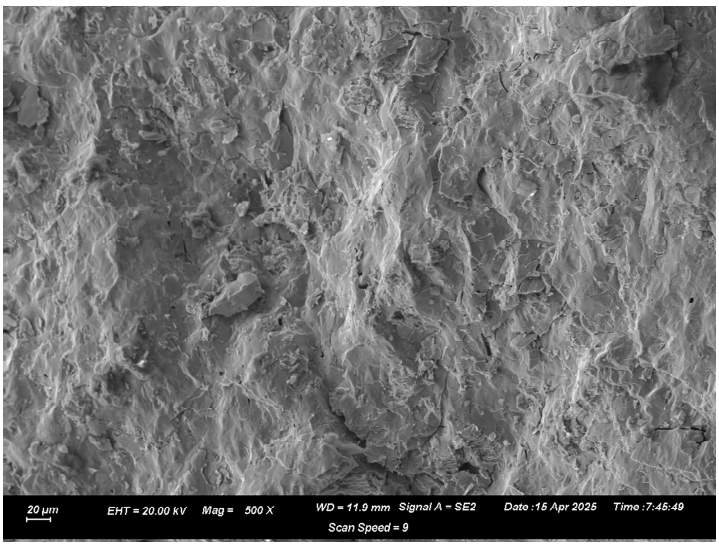


(**a**)

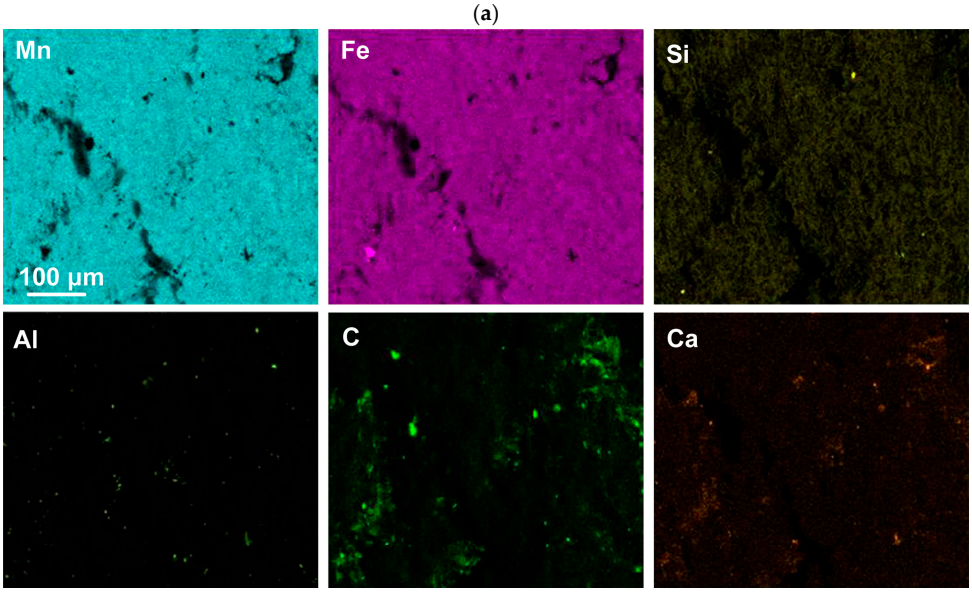


(**b**)

**Figure 2.** (**a**): SEM image (×500) of analysed area (number 1) in Sample A; (**b**): EDX map of area in (**a**).

**Table 4.** EDS analyses of Sample A alloy (mass%); n.a. = not available; n.d. = not detected.

| Area | %Al | %Si | %Mn | %Fe | %Ca | %V | %S | %C |
|---|---|---|---|---|---|---|---|---|
| 1 | 0.6 | 2.4 | 69.4 | 26.9 | 0.1 | 0.6 | 0.0 | n.a. |
| 2 | 0.0 | 2.2 | 68.8 | 28.3 | 0.2 | 0.6 | 0.0 | n.a. |
| 3 | 1.6 | 2.3 | 68.2 | 27.0 | 0.2 | 0.6 | 0.0 | n.a. |
| 4 | 0.8 | 2.1 | 68.1 | 28.3 | 0.1 | 0.6 | 0.0 | n.a. |
| 5 | 1.4 | 1.8 | 67.5 | 28.6 | 0.2 | 0.6 | 0.0 | n.a. |
| Average | 0.9 | 2.2 | 68.4 | 27.8 | 0.2 | 0.6 | 0.0 | n.a. |
| Maximum σ | 0.01 | 0.01 | 0.06 | 0.03 | 0.00 | 0.01 | n.d. | |
| Bulk Alloy | 0.4 | 1.4 | 66.1 | 28.0 | 0.05 | 0.40 | 0.03 | 3.5 |

**Table 5.** EDS analyses of Sample D alloy (mass%); n.a. = not available; n.d. = not detected.

| Area | %Al | %Si | %Mn | %Fe | %Ca | %Cr | %S | %C |
|---|---|---|---|---|---|---|---|---|
| 6 | 1.2 | 2.3 | 56.5 | 18.2 | 0.1 | 21.7 | 0.0 | n.a. |
| 7 | 1.1 | 2.2 | 57.1 | 18.4 | 0.1 | 21.1 | 0.0 | n.a. |
| 8 | 1.1 | 2.2 | 57.3 | 18.5 | 0.1 | 20.7 | 0.0 | n.a. |
| 9 | 1.1 | 2.3 | 57.1 | 18.7 | 0.1 | 20.7 | 0.0 | n.a. |
| 10 | 1.1 | 2.0 | 57.4 | 18.0 | 0.0 | 21.3 | 0.0 | n.a. |
| 11 | 1.4 | 2.7 | 56.4 | 18.5 | 0.0 | 20.9 | 0.0 | n.a. |
| Average | 1.2 | 2.3 | 57.0 | 18.4 | 0.1 | 21.1 | 0.0 | n.a. |
| Maximum σ | 0.01 | 0.01 | 0.06 | 0.03 | 0.01 | 0.03 | n.d. | |
| Bulk Alloy | 1.5 | 3.4 | 56.8 | 18.2 | 0.02 | 17.7 | 0.12 | 2.2 |

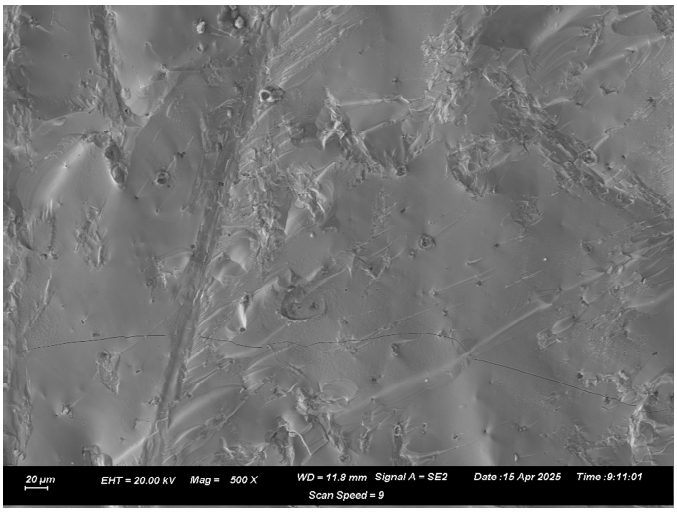


(**a**)

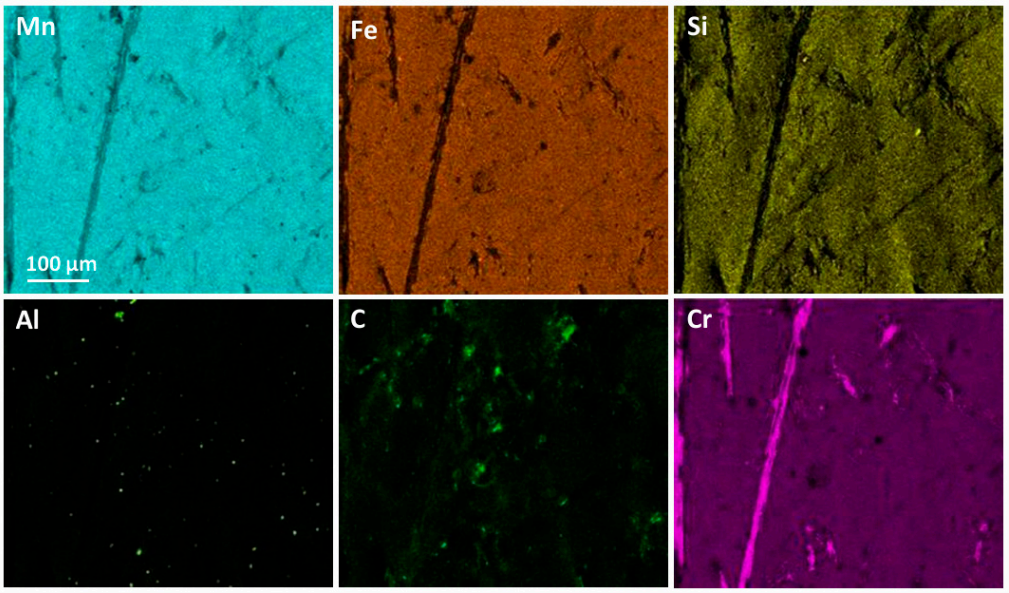


(**b**)

**Figure 3.** (**a**): SEM image (×500) of analysed area (number 6) in Sample D; (**b**): EDX map of area in (**a**).

## 4. Discussion

Although aluminothermic reduction is not considered an equilibrium process, the application of equilibrium phase calculations is useful in investigating the effects of different melting points and chemistries of the target and realised slag and alloy compositions [7–9,11]. In the following section, the thermochemical software FactSage 7.3 and Thermo-Calc 2023b are utilised to calculate equilibrium compositions for comparison with the experimental results presented in this work [21,22]. The main reason for not attaining chemical equilibrium in aluminothermic reduction is the high release rate of heat, resulting in short reaction times and thus limited time for process control. In various studies on the application of aluminothermic reduction for different feed materials, it has been demonstrated that the chemical composition and particle size of the feed material significantly influence the aluminothermic reaction rate and extent, thereby determining the maximum attained temperature and the final product proportions and chemistries [11–14,23,24].

In addition, laboratory studies vary in the reaction atmosphere applied. In some studies, the mixture is reacted under a protective gas atmosphere, such as Argon gas, to

eliminate oxygen in the air from reacting with the feed mixture [7–11]. However, it has been shown that some air is required to initiate the reaction in $MnO_2$–Al mixtures since this mixture did not react under Argon gas [14]. In some studies, oxidants other than air may be added deliberately as an additive, or the oxides targeted for the reduction reaction may form the dual purpose of oxidant and metal/alloy product former. Thus, calculating the feed recipe to limit the %Al in the alloy product is not as simple as in most large-scale furnace-based processes since Al is highly reactive to all oxygen sources.

### *4.1. Alloy Composition*

The sample D Cr-Mn-Fe-Si complex alloy has a relatively low %C at 2.2, similar to a MCFeCr alloy in Table 1. In comparison, the sample A alloy contains 3.5% C. Although both ferrochromium and ferromanganese have a high carbon solubility capacity, the presence of silicon in the alloys decreases the solubility limit of carbon [1]. This effect appears to be at play in both alloys A and D at 1.4 and 3.4% Si, respectively. The carbon saturation level for sample A alloy at 1550 °C is 6.5% C, and for the chromium-containing sample D alloy with a higher %Si, the carbon saturation level is 6.9% C. This is compared to the %C shown in Tables 4 and 5, at 3.5% C in sample A alloy and 2.2% C in sample D alloy.

The equilibrium phase chemistry of the bulk alloy compositions in Tables 4 and 5 is shown in Figure 4. In Figure 4a, the sample A alloy has a solidus temperature of 1093 °C and a liquidus temperature of 1171 °C. The closeness of these two temperatures results in a narrow solidification temperature range, leading to a rapid setting of the alloy composition. The low liquidus and solidus temperatures, relative to the high temperatures attained in aluminothermic reduction, which can easily reach 3000 °C, allow for an extensive alloy separation time [24]. The rapid incorporation of the added chromium metal powders indicates that the aluminothermic reaction temperature was sufficiently high to melt the chromium metal, which has a melting point of 1857 °C. As shown in Figure 4b, the solidus temperature of the sample D alloy is 1026 °C, and the liquidus temperature is 1373 °C. The higher liquidus temperature compared to the sample A liquidus temperature may work against effective bulk alloy separation in sample D.

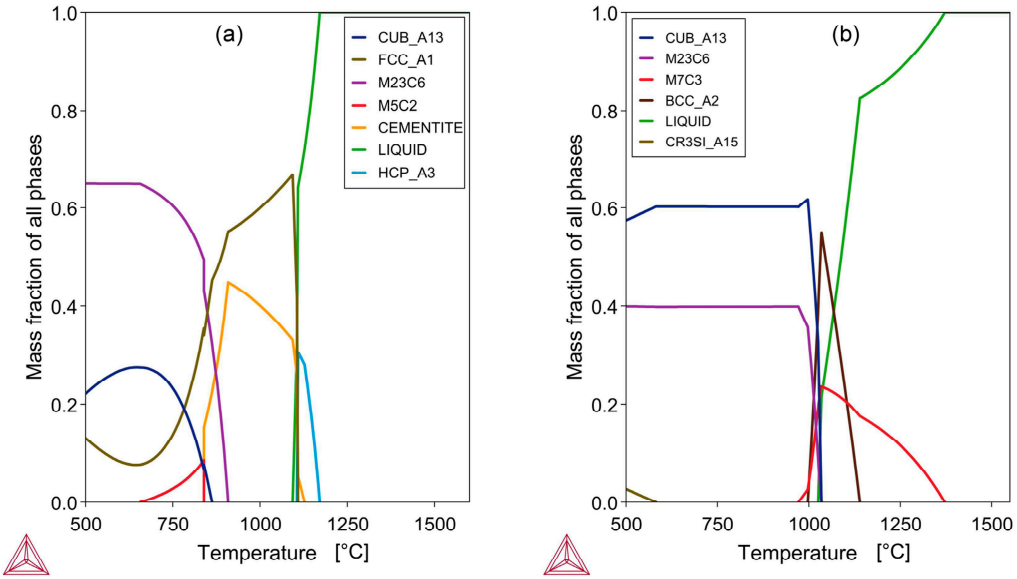


**Figure 4.** Phase chemistry of alloy: (**a**) Sample A alloy; (**b**) Sample D alloy: Calculated in Thermo-Calc [21].

### *4.2. Slag Composition*

The aim slag composition was selected to maintain a low liquidus temperature in the slag, even as a high level of $Al_2O_3$ uptake occurs from aluminothermic reduction reactions, such as reaction (1):

$$3(MnO) + 2(Al) = <Al_2O_3> + 3(Mn) \quad (1)$$

< > = solid; ( ) = liquid

Comparison of the average SEM-EDX slag analyses and bulk slag analyses in Table 6 indicates some alloy entrapment because zero iron content is expected in the slag due to the highly reducing conditions in aluminothermic smelting. Especially for sample D, with added Cr metal, the Cr in the slag is likely metallic, as confirmed by the SEM-EDX analyses in which no Cr-oxide was detected. Mass balance calculations based on the input masses and the output masses of slag and alloy indicate that the alloy mass in the slag and the overall alloy recovery numbers are as shown in Table 7. A comparison of the numbers for sample A versus sample D, at 43% versus 68% alloy yield, indicates that the addition of Cr as a collector metal served its intended purpose, increasing alloy collection and separation. Element accounting percentages shown in Table 8 indicate a good accounting of Fe and Cr, with some loss of Mn, Si, and Al to the gas due to volatilisation of metals at the high reaction temperatures expected in thermic reduction. At an industrial scale, various typical gas- and particulate-capturing equipment options are available, such as a reaction chamber hood with a positive off-gas pressure to counter volatilisation and capture fumes for recycling [3].

**Table 6.** Target vs. test slag analyses (SEM Average) and bulk chemistry.

| | %$Al_2O_3$ | %$SiO_2$ | %MnO | %FeO | %CaO | %$Na_2O$ | %BaO | %CrO | B2 = %CaO/%$SiO_2$ |
|---|---|---|---|---|---|---|---|---|---|
| Target slag | 39 | 17 | 14 | 0.0 | 17 | 11 | 2 | 0 | 1.0 |
| A: EDX | 54.5 | 9.1 | 20.0 | 0.0 | 8.0 | 5.5 | 2.8 | 0 | 0.9 |
| A: bulk | 53.2 | 12.3 | 27.6 | 2.4 | 7.1 | 4.6 | 1.5 | 0 | 0.6 |
| A: Corrected | 52.1 | 11.9 | 22.7 | 0.0 | 7.0 | 4.5 | 1.5 | 0 | 0.6 |
| D: EDX | 59.3 | 9.0 | 12.6 | 0.0 | 10.5 | 6.0 | 2.7 | 0 | 1.2 |
| D: bulk | 51.0 | 11.0 | 26.5 | 3.1 | 9.3 | 4.8 | 1.5 | 4.5 | 0.8 |
| D: Corrected | 54.7 | 10.7 | 17.5 | 0.0 | 10.0 | 5.1 | 1.6 | 0.0 | 0.9 |

**Table 7.** Mass balance numbers (grams unless indicated differently).

| | Alloy | Mn in Alloy | Fe in Alloy | Slag | Fe in Slag | Alloy in Slag | Mn in Ore | Fe in Ore | Mn+Fe +Cr | %Alloy Yield |
|---|---|---|---|---|---|---|---|---|---|---|
| A | 18.7 | 12.4 | 5.3 | 79.1 | 1.5 | 5.3 | 47.7 | 8.3 | 56.0 | 43 |
| D | 30.6 | 17.4 | 5.6 | 106.8 | 2.5 | 13.9 | 47.7 | 8.3 | 66.0 | 68 |

**Table 8.** Mass accounting of primary elements (percent).

| | %Fe | %Mn | %Si | %Al | %Cr |
|---|---|---|---|---|---|
| Sample A | 81 | 67 | 58 | 62 | none |
| Sample D | 97 | 82 | 78 | 80 | 91 |

Comparison of the SEM-EDX slag analyses with the target analysis in Table 6 reveals lower percentages of CaO and $Na_2O$, and higher levels of $Al_2O_3$, in the experimental results. The effect of this higher $Al_2O_3$ content on the slag phase chemistry was investigated by comparing the slag phase chemistry of slag D to that of the target slag.

The cooling curve of the target slag is shown in Figure 5a. It is seen that the slag liquidus temperature is 1373 °C. The slag solidus is relatively low at 1002 °C, allowing ample time for the alloy to separate from the slag upon cooling. The cooling curve for the EDX analysis of slag D from Table 6 is shown in Figure 5b, indicating the formation of spinel and corundum precipitation phases upon cooling. The liquidus temperature is 1647 °C. Therefore, for good slag and alloy separation, the reaction mass temperature must be at least

close to the liquidus temperature. As discussed in [16], the post-tap slag can be modified with additional $Na_2O$-flux to attain the desired slag phase chemistry, with a high $NaAlO_2$ phase content, since high residual heat content remains after the aluminothermic reaction.

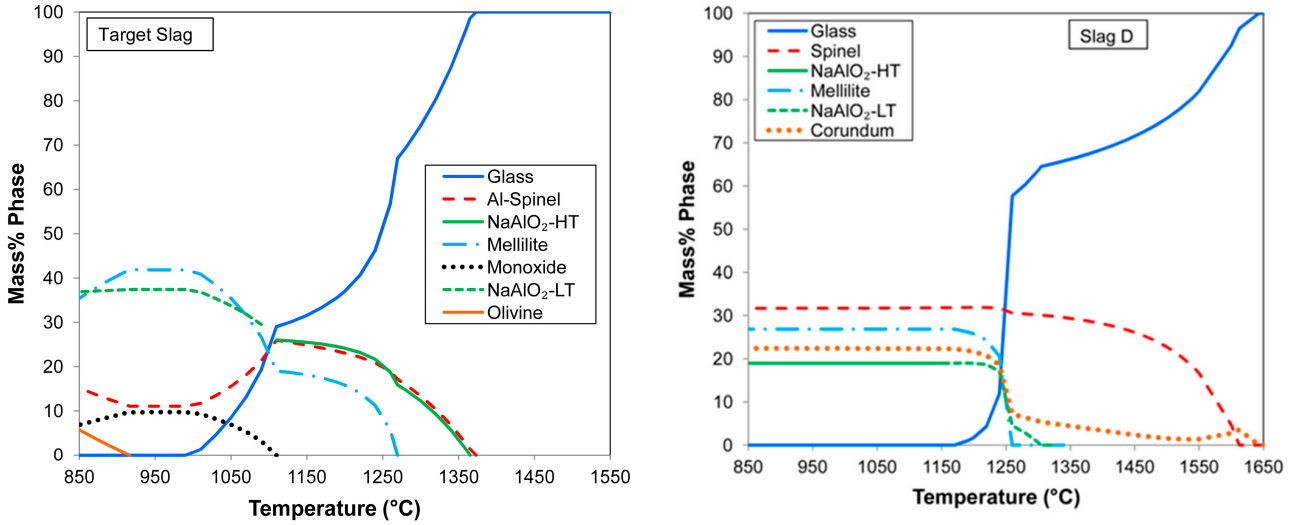


(**a**) (**b**)

**Figure 5.** (**a**): Target slag phase chemistry calculated in FactSage [22]. (**b**): Slag D phase chemistry calculated in FactSage [22].

### *4.3. Gas–Slag–Metal Equilibrium Thermochemistry*

Chemical equilibrium is not expected in the aluminothermic reduction process because of the rapid heat release from aluminium oxidation. To test this expectation, a thermochemistry analysis was conducted. The gas–slag–metal equilibrium for the feed mixture inputs was calculated at temperatures of 1650 °C to 1900 °C. The calculated equilibrium end-point alloy and slag analyses are compared to the experimentally determined values as shown in Figure 6a–d. It is observed that the alloy compositions of %Mn, %Cr, and %Fe are close to equilibrium at 1900 °C. However, the reductant species of %Al, %Si, and %C differ significantly from their equilibrium values at 1900 °C. Especially, the %Al is predicted to be close to zero at equilibrium, whilst this is not the case in the produced alloy. Although a limited quantity of carbon is added to the feed mixture, it is seen in Figure 6a that the equilibrium alloy carbon content varies widely from 4.4% C at 1650 °C to 1.4% C at 1900 °C. Figure 6a also shows the inverse relationship between %C and %Si.

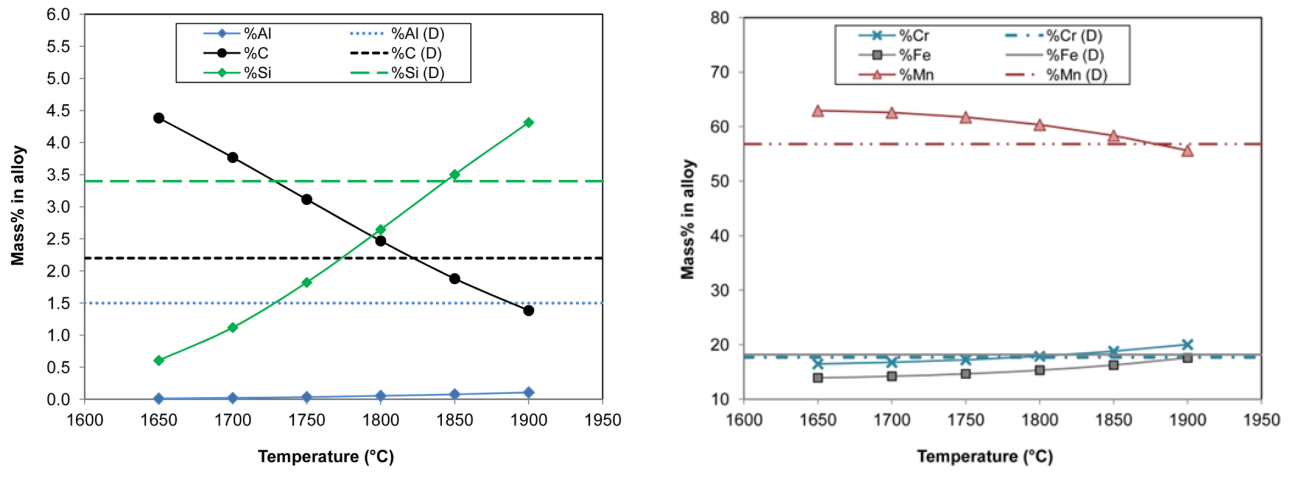


(**a**) (**b**)

**Figure 6.** *Cont.*

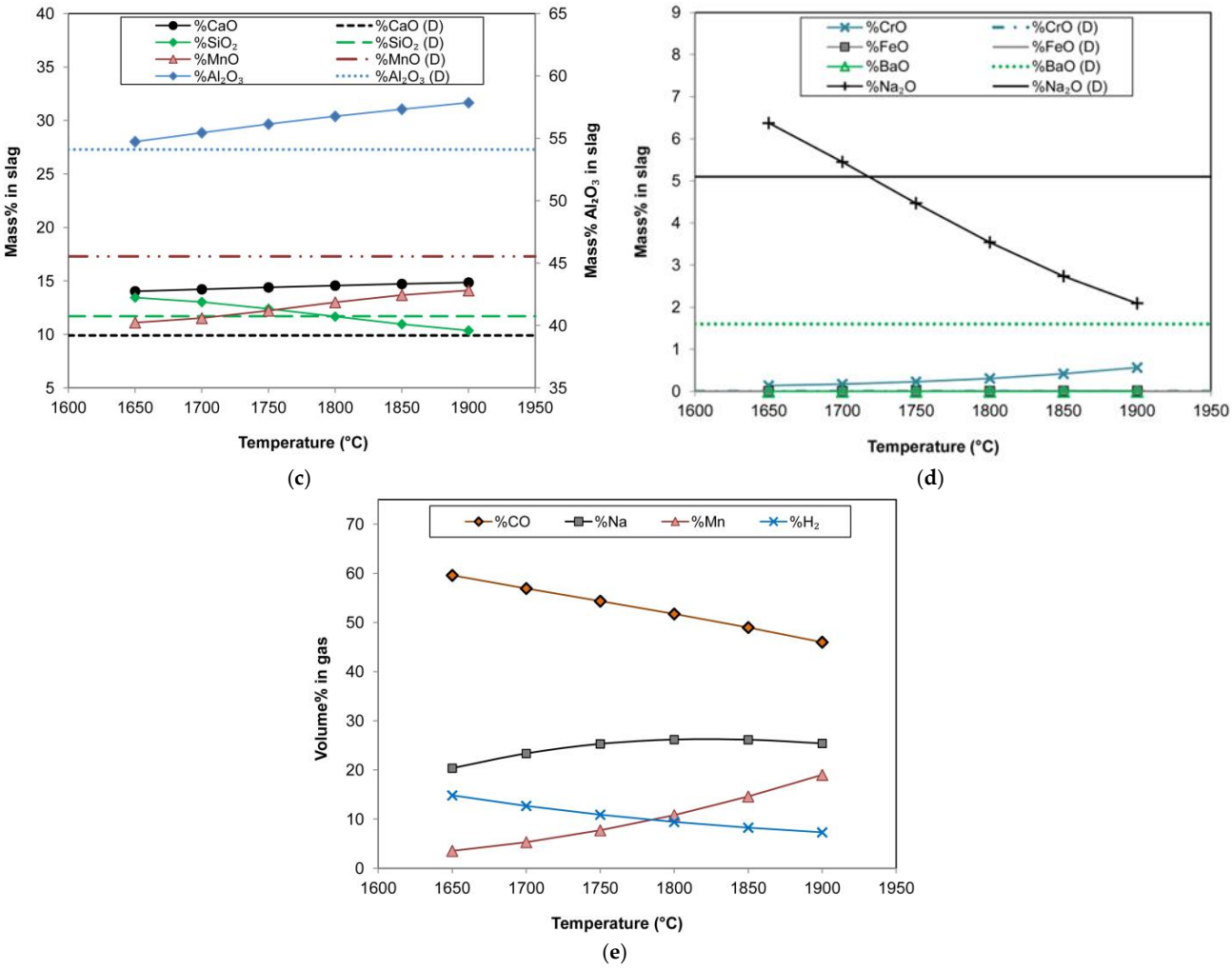


**Figure 6.** (**a**): Sample D alloy composition vs. gas–slag–metal equilibrium. (**b**): Sample D alloy composition vs. gas–slag–metal equilibrium. (**c**): Sample D slag composition vs. gas–slag–metal equilibrium. (**d**): Sample D slag composition vs. gas–slag–metal equilibrium. (**e**): Sample D gas in gas–slag–metal equilibrium from FactSage [22].

The slag analyses displayed in Figure 6c,d show larger differences between equilibrium-predicted values and the experimentally measured values, in large part due to the total oxidation of Al predicted in the equilibrium calculations, as well as the reduction of BaO into the alloy. In addition, the equilibrium calculations predicted a significant loss of Na to the gas phase, whilst the experimental loss appears to be much less. This is a crucial aspect to be able to retain sufficient $Na_2O$ in the slag for fluxing, enabling adequate alloy–slag separation. The main gas compounds are summarised in Figure 6e, which predicts gas-phase losses of Na and Mn. As already mentioned above, the process application on an industrial scale opens equipment possibilities such as the off-gas system and positive furnace pressure control to limit and capture volatiles. In addition, at an industrial scale, a semi-continuous loading procedure is possible, which lowers top temperatures and facilitates the capture of volatiles in the reaction mixture [3].

The gas–slag–metal equilibrium calculation results shown in Figure 6 correspond somewhat to the empirically determined results of alloy and slag chemistry. However, a crucial discrepancy arises from the 1.5% Al observed in the experiment alloy product, which was not predicted in the equilibrium calculations. The reason for this difference is most likely the dwindling chemical reaction driving force as the reaction completion is approached, according to Le Chatelier's principle. The carbothermic reduction of MnO

from slag does not reach equilibrium and depends on the activity differential between the MnO in the reactant phase and the equilibrium MnO activity value. The reaction interface area is the primary uncertain variable [25]. The ore contains limited fluxing compounds, and, therefore, the activity of MnO will be close to unity, as MnO has a high melting point of 1945 °C, and will require time to dissolve into the added flux compounds. To illustrate the likely activity ranges at the start and end of the aluminothermy process, the activity values are presented in Table 9 for a temperature of 1900 °C. The oxide melt was calculated as a mixture of ore and flux compounds forming a high-MnO slag with a liquidus temperature calculated as 1730 °C, resulting in the following composition: 58.9% MnO, 14.5% $SiO_2$, 14.5% CaO, 2.5% $Al_2O_3$, 9.6% $Na_2O$. It is observed that the chemical driving force for reaction (1) is high, as the initial activities of the reactants, Al and MnO, are significantly higher than their equilibrium activity values. The formation of $Al_2O_3$ diffusion barriers on the surface of aluminium particles, either solid or molten, is unlikely in this reaction system because the fluxing agents were explicitly selected to form a slag with high $Al_2O_3$ solubility. Even in the absence of a slag product, it was shown that a continuous $Al_2O_3$ product layer could not form in aluminothermy of granular materials [26].

**Table 9.** Activities in slag and alloy at 1900 °C (liquid reference state).

| | $Al_2O_3$ | MnO | $SiO_2$ | Al | Mn | Si |
|---|---|---|---|---|---|---|
| Oxide melt | $3.46 \times 10^{-5}$ | 0.748 | $7.62 \times 10^{-4}$ | 1.0 | <<0.0001 | <<0.0001 |
| Equilibrium | 0.317 | 0.084 | $8.90 \times 10^{-3}$ | $1.12 \times 10^{-3}$ | 0.484 | $2.69 \times 10^{-3}$ |

Considering that the gas–slag–metal equilibrium calculations were made for a closed system with no air added as reactant, it is clear that the equilibrium calculation may provide, at best, a ballpark number for the required Al addition mass. To illustrate this effect, a gas–slag–metal equilibrium calculation was performed at 1900 °C for different Al reductant addition levels, ranging from ±20% to the experimental value of 30 g of Al, corresponding to 24 g and 36 g of Al addition. The equilibrium calculation results are summarised in Figure 7a,b as the equilibrium alloy and slag compositions.

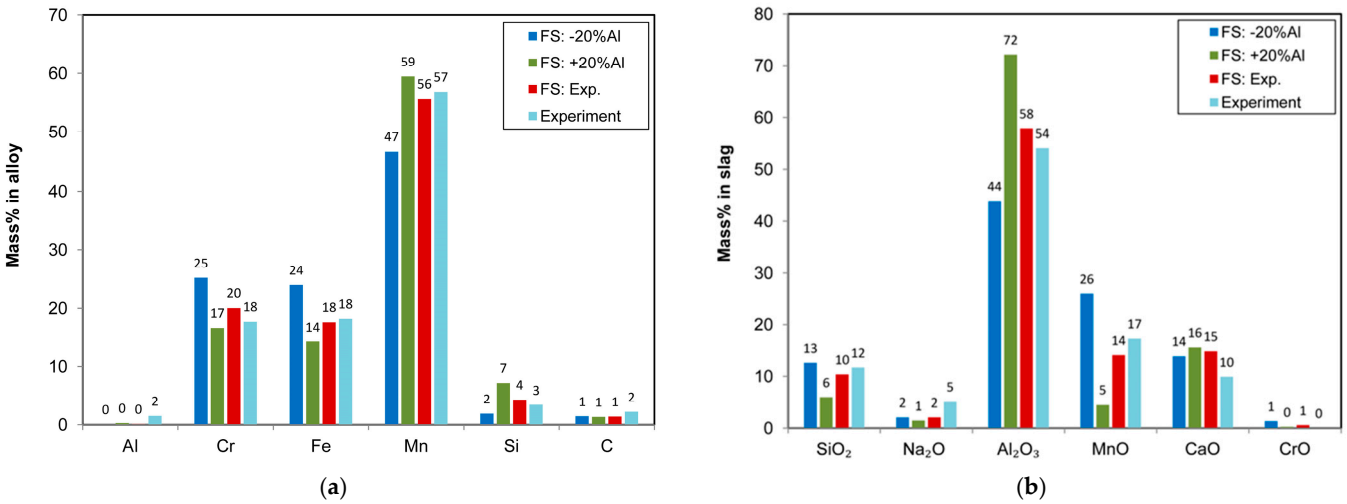


(**a**) (**b**)

**Figure 7.** (**a**): Experimental vs. equilibrium alloy compositions at different Al levels (1900 °C). (**b**): Experimental vs. equilibrium slag compositions at different Al levels (1900 °C).

Figure 7a indicates that, in the equilibrium calculation, all Al metal is reacted with MnO and $SiO_2$, irrespective of the grams of Al added in the range considered here. This effect is clearly visible with 7% Si in the alloy when +20% Al is added. The attendant change in slag composition is drastic, as shown in Figure 7b, indicating an excessively increased $Al_2O_3$

content to 72% and a lowered $SiO_2$ content to 6%, likely resulting in a slag of low fluidity. Therefore, the equilibrium calculation is only useful following experimental verification and may provide trends in chemical changes for estimated temperatures. Precise recipe calculation seems unlikely.

In summary, it is clear from this work that the applied sodium-fluxed slag is a practical approach to enable good alloy–slag separation from one-step aluminothermic reduction of manganese ore with chromium metal as collector metal. A medium-carbon complex alloy of Mn-Cr-Fe-Si can be produced through a reaction design, and the resulting suitable sodium-fluxed high-alumina slag can be used for circular processing to recover aluminium for the Hall–Héroult electrochemical process.

## 5. Conclusions

This work demonstrates the empirical application of a sodium-fluxed aluminothermic reduction system for $MnO_2$-type ores in a single step. The addition of a small quantity of coal as a reductant facilitates rapid pre-reduction to the MnO level, thereby eliminating the need for an extra step of pre-roasting the $MnO_2$ ore.

Chromium metal is used as a collector metal to increase the alloy yield to 68%, from 43% in the absence of the chromium collector metal. The chromium collector metal improved alloy–slag separation. The medium-carbon complex alloy product contains 57% Mn, 18%Cr, 18% Fe, 3.4% Si, 1.5% Al, and 2.2% C. This Mn-Cr containing complex alloy can be applied as an efficient alloying addition in steelmaking because it melts at a lower temperature than MCFeCr of the same carbon content (2.2%C).

The applied $Na_2O$-fluxed feed mixture formulation enables the formation of the water-soluble $NaAlO_2$ compound, allowing for the recycling of $Al_2O_3$ through hydrometallurgical processing via the Bayer process, to the Hall–Héroult electrochemical process, which is used to produce aluminium.

Gas–slag–metal equilibrium calculations show that precise recipe calculation is not achieved through such calculations because the Al reactant requirement does not precisely follow equilibrium. The equilibrium calculations provide temperature estimates and trends in chemical changes. Therefore, theoretical feed mixture formulations must be tested through empirical applications as shown in this work.

**Author Contributions:** F.D.B. conceptualised the work; F.D.B. and T.C. executed the experiments together, interpreted the data together, and prepared the manuscript together. All authors have read and agreed to the published version of the manuscript.

**Funding:** This research was funded in part by the University of Pretoria.

**Data Availability Statement:** The original contributions presented in this study are included in the article. Further inquiries can be directed to the corresponding author.

**Acknowledgments:** The authors are grateful to Coenraad Snyman at the Laboratory for Microscopy and Microanalysis at the University of Pretoria for his advice and assistance on the SEM imaging and analysis in this work.

**Conflicts of Interest:** The authors declare no conflicts of interest. The funders had no role in the design of the study; in the collection, analyses, or interpretation of data; in the writing of the manuscript, or in the decision to publish the results.

## Abbreviations

The following abbreviations are used in this manuscript:

| | |
|---|---|
| HCFeCr | High–carbon ferrochromium |
| MCFeCr | Medium-carbon ferrochromium |
| LCFeCr | Low-Carbon ferrochromium |
| FeCrMn | Ferrochrome-manganese |
| FeCrSiMn | Ferrochrome-siliconmanganese |
| PID | Proportional-integral-derivative |
| SEM | Scanning electron microscope |
| EDX | Energy dispersive X-ray spectroscopy |
| ICP-OES | Inductively coupled plasma optical emission spectroscopy |
| XRF | X-ray fluorescence |

## References


1. Habashi, F. (Ed.) *Handbook of Extractive Metallurgy*; Wiley-VCH: Weinheim, Germany, 1997; Volume 1, pp. 420–451.
2. *ASTM A101-80*; Standard Specification for Ferrochromium. ASTM International: West Conshohocken, PA, USA, 1985.
3. Gasik, M. *Handbook of Ferroalloys*; Butterworth-Heinemann: Oxford, UK, 2013; pp. 495–499.
4. Shabanov, Y.; Baisanov, S.; Grigorovich, K.; Baisanova, A.; Toleukadyr, R.; Saulebek, Z. Recovery of low-carbon ferrochrome with multi-component aluminum-silicon-chrome (Al-Si-Cr) alloy. *Metalurgija* **2020**, *59*, 514–516.
5. Makhambetov, Y.; Kutzhanov, M.; Toleukadyr, R.; Myrzagaliyev, A.; Sadyk, Z.; Saulebek, Z.; Akhmetov, A. Utilization of Chromite Spinel Powder in the Metallothermic Smelting of Low-Carbon Ferrochrome. *Processes* **2025**, *13*, 2288. [CrossRef]
6. Andrusev, M.M. 150 Years since the birth of the eminent Russian physical chemist and metallurgist N.N. Beketov. *Metallurgist* **1977**, *21*, 416–418. [CrossRef]
7. Kudyba, A.; Akhtar, S.; Johansen, I.; Safarian, J. Aluminothermic Reduction of Manganese Oxide from Selected MnO-Containing Slags. *Materials* **2021**, *14*, 356. [CrossRef] [PubMed]
8. Kudyba, A.; Safarian, J. Manganese and Aluminium Recovery from Ferromanganese Slag and Al White Dross by a High Temperature Smelting-Reduction Process. *Materials* **2022**, *15*, 405. [CrossRef] [PubMed]
9. Philipson, H.; Wallin, M.; Einarsrud, K.E.; Tranell, G. Kinetics of silicon production by aluminothermic reduction of silica using aluminum and aluminum dross as reductants. In Proceedings of the 16th International Ferro-Alloys Congress (INFACON XVI), Virtual, 27–29 September 2021; NTNU: Trondheim, Norway, 2021.
10. Nababan, D.C.; Mukhlis, R.; Durandet, Y.; Prentice, L.H.; Rickard, W.D.A.; Pownceby, M.I.; Rhamdani, M.A. Recycling of $LiCoO_2$ Battery Cathode Material Through Aluminothermic Reduction Using Aluminum Waste Chips. *Met. Mater. Trans. B* **2024**, *55*, 144–167. [CrossRef]
11. Sparis, D.; Lazou, A.; Balomenos, E.; Panias, D. Thermodynamics of Aluminothermic Processes for Ferrotitanium Alloy Production from Bauxite Residue and Ilmenite. *Metals* **2024**, *14*, 200. [CrossRef]
12. Barsukova, N.V.; Popov, A.V.; Komarov, O.N. Evolution of structure and properties of iron-carbon alloys produced by aluminothermy at differentiation of fractional composition of charge materials. *Metallurgist* **2025**, *68*, 1743–1755. [CrossRef]
13. Barsukova, N.V.; Komarov, O.N.; Zhilin, S.G.; Predein, V.V.; Popov, A.V.; Khudyakova, V.A. Control of Properties of Iron-Carbon Alloys Produced by Aluminothermy by Varying Technological Factors. *Metallurgist* **2023**, *67*, 1192–1207. [CrossRef]
14. Sarangi, B.; Sarangi, A.; Ray, H.S. Kinetics of aluminothermic reduction of $MnO_2$ and $Fe_2O_3$: A thermoanalytical investigation. *ISIJ Int.* **1996**, *36*, 1135–1141. [CrossRef]
15. Bhoi, B.; Murthy, B.V.R.; Datta, P.; Rajeev; Jouhari, A.K. Studies on Aluminothermic Reduction of Manganese ore for Ferro Manganese Making. In *Proceeding: Ferro Alloy Industries in the Liberalised Economy*; Vatsh, A.K., Singh, S.D., Goswami, N.G., Ramachandrarao, P., Eds.; NML: Jainshedpur, India, 1997; pp. 66–70.
16. Coetsee, T.; De Bruin, F. Sodium Oxide-Fluxed Aluminothermic Reduction of Manganese Ore with Synergistic Effects of C and Si Reductants: SEM Study and Phase Stability Calculations. *Reactions* **2025**, *6*, 40. [CrossRef]
17. Makhambetov, Y.; Gabdullin, S.; Zhakan, A.; Saulebek, Z.; Akhmetov, A.; Zulhan, Z.; Mukanov, S. Production of complex Fe-Si-Mn-Cr ferroalloy using high-ash coal: A sustainable metallurgical approach. *Mater. Res. Express* **2024**, *11*, 056523. [CrossRef]
18. Azof, F.I.; Safarian, J. Leaching kinetics and mechanism of slag produced from smelting-reduction of bauxite for alumina recovery. *Hydrometallurgy* **2020**, *195*, 105388. [CrossRef]
19. Pilla, G.; Hertel, T.; Pontikes, Y. Toward an integrated and sustainable Bauxite residue valorization, employing $H_2$ reduction roasting, carbonation, and bio-carbon smelting. *J. Sustain. Metall.* **2025**, *11*, 1745–1765. [CrossRef]

20. *SANS 17246:2011*; South African National Standard Coal-Proximate Analysos. SABS Standards Division: Pretoria, South Africa, 2011.
21. Andersson, J.-O.; Helander, T.; Höglund, L.; Shi, P.; Sundman, B. Thermo-Calc & DICTRA, computational tools for materials science. *Calphad* **2002**, *26*, 273–312. [CrossRef]
22. Bale, C.W.; Bélisle, E.; Chartrand, P.; Decterov, S.A.; Eriksson, G.; Gheribi, A.E.; Hack, K.; Jung, I.-H.; Kang, Y.-B.; Melançon, J.; et al. FactSage thermochemical software and databases, 2010–2016. *Calphad* **2016**, *54*, 35–53; reprinted in *Calphad* **2016**, *55*, 1–19. [CrossRef]
23. Behera, R.C.; Mohanty, U.K. Effect of oxide fluxes on the viscosity of molten aluminothermic ferro-chrome slags. *ISIJ Int.* **2001**, *41*, 827–833. [CrossRef]
24. Branzei, M.; Cojocaru, M.O.; Coman, T.A.; Vascan, O. A model of optimization and control the thermite kit for aluminothermic welding. *Solid State Phenom.* **2016**, *254*, 83–90. [CrossRef]
25. Olsφ, V.; Tangstad, M.; Olsen, S.E. Reduction kinetics of MnO-saturated slags. In Proceedings of the INFACON 8, The Chinese Society of Metals, Beijing, China, 7–10 June 1998; pp. 279–283.
26. Yang, J.; Kuwabara, M.; Sawada, T.; Sano, M. Kinetics of isothermal reduction of MgO with Al. *ISIJ Int.* **2006**, *46*, 1130–1136. [CrossRef]